Author/s:
Wen, D;Crozier, KB

Title:
Metasurfaces 2.0: Laser-integrated and with vector field control

Date:
2021-08-01

Citation:
Wen, D. & Crozier, K. B. (2021). Metasurfaces 2.0: Laser-integrated and with vector field control. APL Photonics, 6 (8), https://doi.org/10.1063/5.0057904.

Persistent Link:
https://hdl.handle.net/11343/289581

APL Photonics

Metasurfaces 2.0: Laser-integrated and with vector field control

Cite as: APL Photonics **6**, 080902 (2021); https://doi.org/10.1063/5.0057904
Submitted: 25 May 2021 • Accepted: 03 August 2021 • Published Online: 16 August 2021

Dandan Wen and Kenneth B. Crozier

Metasurfaces 2.0: Laser-integrated and with vector field control

Cite as: APL Photon. 6, 080902 (2021); doi: 10.1063/5.0057904
Submitted: 25 May 2021 • Accepted: 3 August 2021 •
Published Online: 16 August 2021

Dandan Wen[1,2] and Kenneth B. Crozier[2,3,4,a)]

AFFILIATIONS

[1] Key Laboratory of Light Field Manipulation and Information Acquisition, Ministry of Industry and Information Technology, and Shaanxi Key Laboratory of Optical Information Technology, School of Physical Science and Technology, Northwestern Polytechnical University, Xi'an 710129, China
[2] Department of Electrical and Electronic Engineering, University of Melbourne, Victoria 3010, Australia
[3] School of Physics, University of Melbourne, Victoria 3010, Australia
[4] Australian Research Council (ARC) Centre of Excellence for Transformative Meta-Optical Systems, University of Melbourne, Victoria 3010, Australia

[a)] **Author to whom correspondence should be addressed:** kcrozier@unimelb.edu.au

ABSTRACT

The past decade has witnessed the rapid development of metasurfaces. In this paper, we outline our thinking on what we regard as two important trends in metasurface research, namely, the continual improvement in the light field modulation capacity of metasurfaces and the integration of metasurfaces with other devices to achieve fully contained optical systems. We first describe one of the fastest growing branches of the former, which is known as metasurface-based vectorial holography. This aims to control the wavefront and the polarization state of a light beam simultaneously. In comparison with single function devices, i.e., those that modulate the wavefront or polarization but not both, metasurface vectorial holography represents a significant improvement in our ability to modulate light fields. We then discuss the integration of metasurfaces with lasers for the goal of direct modulation of the polarization of the output beam or for the generation of beams with tailored orbital angular momenta. Two methods for doing so are discussed, namely, on-facet integration and in-cavity integration. We hope this Perspective will provide readers with new insights and thus help extend applications of metasurface-based optical devices.

I. INTRODUCTION

Representing the two-dimensional (2D) counterpart of metamaterials, metasurfaces consist of one or a few layers of nanostructures that locally change the properties of incident waves. The past decade has witnessed fast progress in metasurface development, largely driven by potential industry applications and by curiosity-driven scientific research. Metasurface can be fabricated with standard nanofabrication processes, such as electron beam lithography (EBL), focused ion beam (FIB), and deep-ultraviolet (DUV) lithography. Indeed, the necessary fabrication processes are generally much less complex than those needed for three dimensional (3D) metamaterials. Metasurfaces such as reflection-mode metal–dielectric–metal metasurfaces[1] and transmission-mode dielectric metasurfaces[2] have also been shown to offer high efficiency, facilitating their use in practical applications.

In the early stages of metasurface research, it was common to only modulate one property of the light field. Examples include phase-only holograms,[3] lenses,[4] and waveplates.[5] With progress in design methods and fabrication techniques, researchers started to develop metasurfaces that simultaneously modify multiple properties of the light field (Fig. 1). An example is the simultaneous modulation of phase and transmission (or reflection) spectra. Lim *et al.*[6] demonstrated a holographic color print that appears as a color image under white light while projecting multiple holographic images when illuminated by red, green, or blue laser beams. Similar spectral/phase modulation have also been realized by Wen *et al.*,[7] Wei *et al.*,[8] Bao *et al.*,[9] and Zhang *et al.*[10] Other functions include the combined control of the high harmonic generation/phase,[11] amplitude/phase,[12–14] phase/polarization,[15] and many more.[16–18]

Another trend has been as follows: Most early metasurfaces were designed to work as independent elements, taking an input

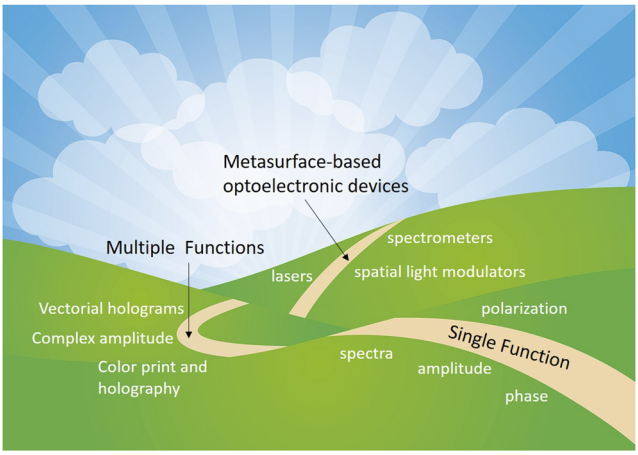

FIG. 1. Roadmap of metasurfaces.

Gaussian beam or plane wave and modulating its properties to produce an output beam or wave that propagates in free space. There has been a trend toward integrating metasurfaces with other devices to achieve fully contained optical systems. Some examples are as follows: Meng *et al.* used a metasurface array comprising silicon nanowire photodetectors of different diameters as a visible-wavelength microspectrometer.[19] In the area of microelectromechanical systems (MEMS), metasurfaces have been integrated with atomic force microscope cantilevers to improve the optical lever sensitivity.[20] The integration of metasurfaces in laser cavities or on their output facets has made possible self-contained systems that generate high order Poincaré or vortex beams.[21]

In this Perspective, we outline our thinking on what we regard as two important emerging trends in metasurfaces, namely, metasurfaces known as vectorial holograms that control field distributions and metasurfaces integrated with lasers. This paper is organized as follows: In Sec. II, we introduce the concept of vectorial holography. This represents an efficient way to realize simultaneous polarization and phase control. We will start with the most basic configuration, i.e., a hologram that reconstructs images with orthogonal polarizations. Multichannel vectorial holograms that have three or more polarization channels are then discussed. We conclude by discussing vectorial holograms that achieve continuous polarization distributions. In Sec. III, we describe examples of works that have integrated metasurfaces into lasers. We start from lasers with on-facet metasurfaces. We then discuss those with in-cavity metasurfaces. In Sec. IV, we will conclude the paper with our thoughts on the future development of metasurfaces.

II. METASURFACE-BASED VECTORIAL HOLOGRAPHY

A. Two-channel vectorial holograms with orthogonal polarization states

1. Orthogonal linear polarization

Long before the term "metasurface" became popular in optics, researchers investigated the reconstruction of wavefronts with non-uniform polarization distributions. The most straightforward example is that of devices that impart independent phase profiles to light with orthogonal polarization states. This minimizes crosstalk between the two polarization channels. In 1965, Lohmann[22] performed such a study, entitled "Reconstruction of vectorial wavefronts," using two linear polarization channels. The target image contains one part that is x-polarized and another that is y-polarized. The x- and y-polarized reference beams are inclined and interfere with the x- and y-polarized object waves to form interference fringes A and B, respectively [Fig. 2(a), top panel]. Despite fringes A and B being generated independently, there will be crosstalk images, i.e., fringe A will also act on the y-polarized incident light and form an image, which was originally intended to be x-polarized (but is instead y-polarized). The crosstalk image will take away some of the transmitted power but will be diverted from the designed observation zone via the use of an off-axis design [Fig. 2(a), bottom panel]. The desired vectorial wavefront will thus be reconstructed.

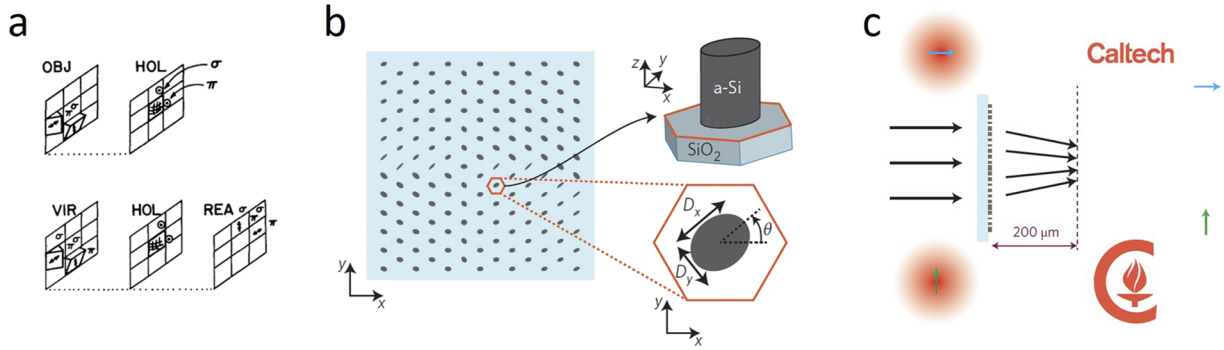

FIG. 2. (a) Holography of a vectorial wavefront. Top panel: recording process. OBJ: object to be recorded. Here, the object contains two parts—π and σ—of orthogonal linear polarizations. Two prisms are used to provide inclined reference beams with orthogonal linear polarizations. HOL: hologram. Bottom panel: reconstruction process. VIR: virtual image plane. REA: real image plane. (b) The schematic of the metasurface and its unit cell. (c) The polarization-switchable metasurface that generates two independent images for x- and y-polarized incident light. Figure (a) is reproduced with permission from Appl. Opt. **4**, 1667–1668 (1965). Copyright 1965 The Optical Society. Figures (b) and (c) are reproduced with permission from Nat. Nanotechnol. **10**, 937–943 (2015). Copyright 2015 Springer Nature.

Recent years have seen new ways of generating two-channel vectorial holograms. In 2013, Pors *et al.*[23] demonstrated a metasurface comprising a periodic arrangement of metal nanobricks. The complex reflection coefficients for the light polarized along the long and short axes of the nanobricks can be controlled independently, enabling the realization of polarization beam splitters. Chen *et al.*[24] employed a reflection-mode metasurface that contains a gold bottom layer, a MgF_2 spacer, and a gold nano-cross layer (on the top). When the *x*-polarized light illuminates on a nano-cross, it mainly interacts with its horizontal (i.e., *x*-oriented) arm. The phase of the reflected light can thus be controlled by varying the length of this arm. In the same way, the length of the vertical arms controls the phase of the *y*-polarized light. Two independent holograms can therefore be encoded into the same metasurface. Schonbrun *et al.*[25] demonstrated birefringent metasurfaces consisting of elliptical amorphous silicon nanoposts on glass substrates. Each nanopost can be regarded as an elliptical-shaped waveguide, which has different refractive indices for the modes polarized along the two different axes. This means that the phase shifts imposed on the light polarized along the long and short axes of the nanopost (φ_x and φ_y) can be controlled independently. Arbabi *et al.*[15] used this principle for holography [Fig. 2(b)]. As shown in Fig. 2(c), two holographic images are reconstructed by the *x*- and *y*-polarized light, respectively. If φ_x, φ_y, and the rotation angle of a nanopost could be chosen freely, any symmetric and unitary Jones matrix can be achieved by such nanoposts, and therefore, any arbitrary polarization and phase transformation can be performed. For example, focused radially and azimuthally polarized beams can be generated by the *x*- and *y*-linearly polarized incident beams, respectively. Martins *et al.*[26] employed elliptical silicon posts on sapphire substrates for visible-wavelength 3D stereoscopic holography. This is realized when two similar images are reconstructed with orthogonally polarized light and are slightly separated in space.

Xie *et al.*[27] used plasmonic nanoslits as building blocks to realize a polarization-selective detour phase hologram. The position, number, and orientation of the slits determine the phase, amplitude, and polarization direction of the transmitted light, respectively. Two types of slits along the *x*- and *y*-directions are fabricated on the same aluminum substrate, which reconstructs two images of orthogonal polarization in the far field. Similarly, Min *et al.*[28] experimentally demonstrated a nanoslit-based metasurface to generate an optical vortex and an Airy beam with *x*- and *y*-polarized light, respectively.

For the anisotropic nanostructures mentioned above, each unit simultaneously contributes to both orthogonal polarizations. A typical way of doing so involves the generation of two look-up tables. The first describes the relationship between the phase of the *x*-polarized light and the nanostructure geometry, while the second table describes the case for *y*-polarized light.[29–31] If one needs φ_1 and φ_2 for *x*- and *y*-polarized light, respectively, the two tables are referred to for finding the nanostructure producing the closest match to the desired values of φ_1 and φ_2. It might be the case, however, that no nanostructure will exist that produces the desired values of φ_1 and φ_2 (or an acceptable approximation). In contrast, Cheng *et al.*[32] showed that two types of nanoantennas can be spatially interleaved to form one metasurface, with each type only contributing to *x*- or *y*-polarized images. Since the choice of unit cells for each polarization is increased, there will be more phase levels, enabling more accurate sampling of the phase profile.

2. Orthogonal circular polarization

Thus far, we have discussed metasurfaces that manipulate linear polarizations. In this section, we discuss metasurfaces that instead use a circular polarization basis, i.e., left circularly polarized (LCP) and right circularly polarized (RCP) light. Early works refer to this approach as "polarization-holographic multiplexing" and usually involve materials that respond to the polarization of light, such as azobenzene and azobenzene-containing polymers. Todorov *et al.*[33] demonstrated a polarization hologram device that contains two types of interference patterns. The first is generated by an LCP reference wave and an RCP object wave. For the second, the object is changed, and the helicities of the reference and object waves are swapped as well. Two independent holographic images can thus be formed with the LCP and RCP reference waves.

When circularly polarized beam illuminates an anisotropic structure, it can be partly converted into a beam that has opposite helicity and carries a geometric phase. Since the sign of the phase, i.e., positive or negative, is determined by the helicity of the incident light, this approach provides a convenient way for realizing LCP- and RCP-multiplexed metasurface holograms. In 1999, Gori[34] proposed a particular class of polarization grating that shifts RCP and LCP components of the incident light to the +first and −first orders, respectively. Shortly after that, Bomzon *et al.*[35] fabricated a computer-generated subwavelength grating with continuously varied local orientation and period. Performance of this device was verified with a mid-infrared laser beam (wavelength $\lambda = 10.6\,\mu$m). These early works can be regarded as the debut of geometric phase-based two-channel metasurface holograms.

In 2015, Wen *et al.*[36] demonstrated a helicity-multiplexed phase-only hologram. The phase profile of the reflected light from a geometric metasurface is conjugated when the incident light helicity is swapped. Therefore, if it generates an image $I(x, y)$ in the far field under LCP illumination, the image changes into $I(-x, -y)$ when the incident light is RCP. If $I(x, y)$ contains two symmetrically distributed off-axis images, these images will be interchanged when the helicity of the input light is swapped. A similar principle can be used for metasurface-based optical illusion[37] and Orbital angular momentum (OAM) beam superposition.[38] That the hologram is two-channel does not necessarily mean that the number of the reconstructed images is limited to two. In 2015, Huang *et al.*[39] combined the complex amplitudes of several computer-generated holograms to form a hybrid hologram. It reconstructed four independent images, i.e., two LCP images and two RCP images, in different diffraction directions and at different positions. Wei *et al.*[40] used the iterative 3D Fienup algorithm to design a multiplane hologram. Since the hologram works in the Fresnel range, the reconstruction distance is a key parameter, i.e., the correct image can only be reconstructed at the designed distance. When the metasurface is illuminated by the LCP light, four RCP images are reconstructed at four separate distances with little crosstalk between them. By switching the incident light to RCP, four different LCP images will appear at the same positions.

The concept of helicity multiplexing can be combined with wavelength multiplexing to realize spin-selected multi-color holograms. Wang *et al.*[41] designed a metasurface that incorporates two types of nano-blocks. One type is designed for red illumination, while the other, for green illumination. The red and green

holographic images in the observation zone change with the helicity of the incident light. The color of the superposed image is therefore tunable. Jin *et al.*[42] controlled both the polarization (LCP and RCP) and color (R/G/B) of the incident light beams to realize a 6-bit metasurface hologram, which reconstructs 63 different holographic images in the Fresnel range. Feng *et al.*[43] fabricated a metasurface that contains three types of silicon nanorods that can reconstruct different LCP and RCP 3D holographic images. Zhang *et al.*[44] used a metasurface comprising chromium nanoapertures on a glass substrate. It generates different color holographic images in the transmission and reflection spaces.

Geometric metasurfaces can be used in nonlinear optics for the flexible control of high order harmonic generation.[11,45] For example, split ring antennas can be used for investigating second harmonic generation due to the lack of central symmetry. When a gold split ring antenna (with the orientation angle φ) is illuminated by LCP light, the transmitted fundamental RCP component takes a geometric phase of 2φ. The LCP and RCP second harmonic generation acquire nonlinear geometric phases of φ and 3φ, respectively. Therefore, three beams imparted with different geometric phases can reconstruct three independent holographic images.[46]

3. Arbitrary orthogonal polarization states

As discussed above, most two-channel vectorial holograms employ orthogonal linear or circular polarization states. On the other hand, the use of other orthogonal polarization states including elliptical polarization would expand the scope of what could be achieved with metasurface polarization optics. Balthasar Mueller *et al.*[47] demonstrated a metasurface that uses elliptical TiO_2 pillars to achieve such functionality. The orientation angle θ and the phase shifts ϕ_x and ϕ_y for the light polarized along the two axes of the pillar can be simultaneously controlled, which allows two independent phase profiles for any two orthogonal polarization states. Using a similar principle, Devlin *et al.*[48] experimentally demonstrated that two beams of orthogonal elliptical polarization states can be converted into states with independent values of orbital angular momentum. Guo *et al.*[49] experimentally verified a single metasurface for the generation of vortex knots and links at the microscale.

B. Multi-channel vectorial holograms

Successful demonstration of two-channel vectorial metasurface holograms has paved the way for those with more polarization channels. Zhao *et al.*[50] used a metasurface comprising amorphous silicon pillars (600 nm tall) on a glass substrate [Fig. 3(a)]. The birefringence of each pillar (ϕ_x and ϕ_y as mentioned in II A 3) and its orientation angle θ provide three different phase values (ϕ_1, ϕ_2, and ϕ_3) for x-polarized input/output, y-polarized input/output, and x-polarized input/y-polarized output, respectively. Since the value of ϕ_3 is dependent on ϕ_1 and ϕ_2 by $\phi_3 = 2\phi_2 - \phi_1 + \pi$, a modified Gerchberg–Saxton (GS) method is used to generate the three holographic images desired for the different polarization channels with minimal crosstalk. By controlling the input/output polarization states, each of the three target images can be made to appear or not appear. There are thus eight combinations in total, but this includes the case where no images appear, so there are seven combinations if the latter is excluded. Zhao *et al.* experimentally demonstrated these combinations [Fig. 3(b)].

A similar principle can be applied to realize muti-colour holograms. Hu *et al.*[51] demonstrated a metasurface consisting of TiO_2 rectangular nanopillars on a glass substrate [Fig. 4(a)]. Phase profiles corresponding to the red, green, and blue holographic images are obtained and assigned to different polarization channels. When the incident light and output light are both x-polarized, only the red image is reconstructed. In the same way, x-in/y-out and y-in/y-out generate green and blue images, respectively. Since correct images can only be reconstructed under certain input/output polarization combinations, an optical system that provides the appropriate input/output polarization states for each color channel and then combines the R, G, and B images is needed to form the color holographic vectorial image [Fig. 4(b)].

Deng *et al.*[52] proposed the concept of diatomic metasurfaces for vectorial holography. Each unit cell contains two silver nanorods with perpendicular directions [Fig. 5(a)]. When the metasurface is illuminated at the appropriate angle, the incident light polarized parallel to the nanorod can be more efficiently diffracted into the negative first diffraction order. The displacement of the nanorod pair from the cell center determines the phase of the reflected light, which can be explained by the concept of the detour phase. The distance between the two nanorods in a unit cell and the orientations of the

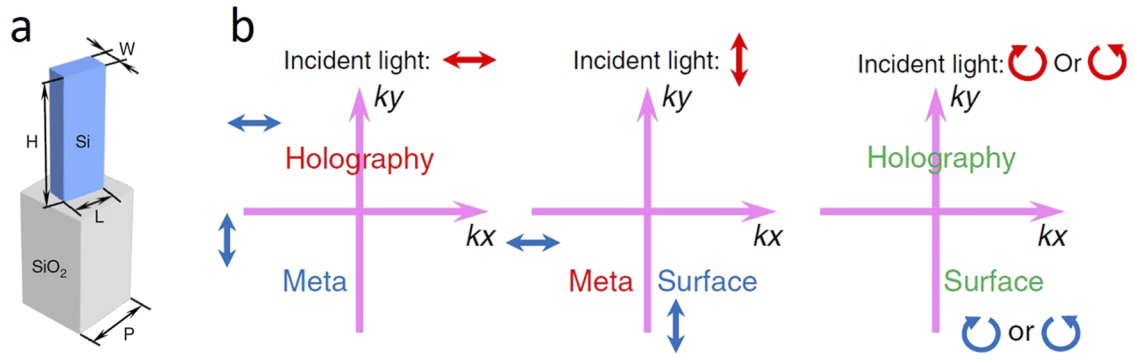

FIG. 3. (a) Schematic of a unit cell. (b) Designed target images of the multichannel polarization multiplexed hologram. Figures are reproduced with permission from Light: Sci. Appl. **7**, 95 (2018). Copyright 2018 Springer Nature.

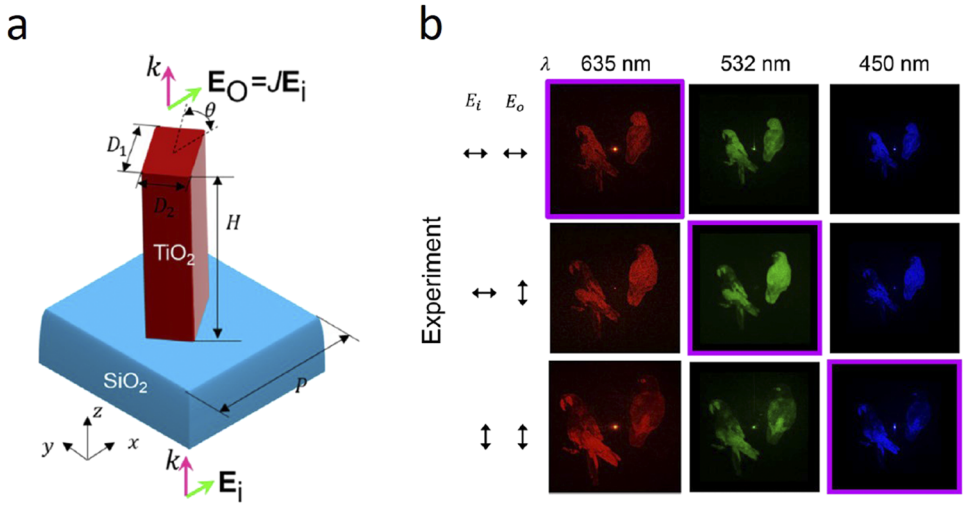

FIG. 4. (a) Schematic of a unit cell. E_i/E_O: electric fields of the input/output light. *J*: Jones matrix of the unit cell. (b) The input/output polarization states (black arrows) and the generated holographic images. Figures are reproduced with permission from Nano Lett. **20**, 994–1002 (2019). Copyright 2019 American Chemical Society.

nanorods can provide full control of the polarization of the reflected light. With this principle, four types of unit cells are combined to form a single metasurface that reconstructs four holographic images of different polarization states [*x*- and *y*-LCP and RCP, Fig. 5(b)].

Song *et al.*[53] demonstrated a metasurface for which the unit cell contains two rows of nanopillars [Fig. 6(a)]. The first and second rows deflect LCP and RCP light, respectively, to a specific direction. By controlling the orientation angles and dimension of the pillars in the two rows, a phase difference and amplitude difference can be formed between the deflected LCP and RCP light, which then superpose and form a beam with a controllable polarization state. Four holographic images with *x*- and 45° linear polarizations and RCP and left-handed elliptical polarization states are experimentally generated [Fig. 6(b)].

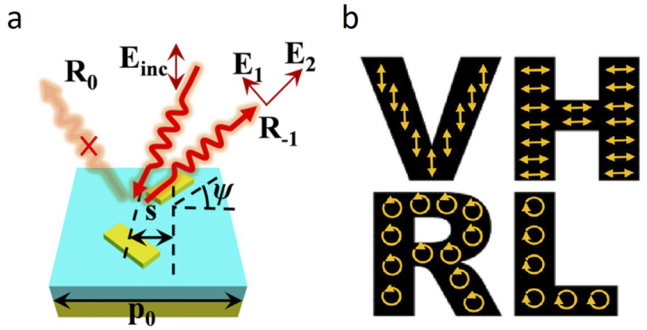

FIG. 5. (a) Schematic of a unit cell of the metasurface. E_{inc}: electric field of the incident light. R_0/R_{-1}: reflectance in the zeroth/negative first diffraction order. E_1/E_2: field components parallel to the bottom/top nanorod in the unit cell. (b) Target holographic images to be generated. Yellow arrows denote the polarization states. Figures are reproduced with permission from Nano Lett. **18**, 2885–2892 (2018). Copyright 2018 American Chemical Society.

C. Continuous vectorial holograms

The works demonstrated above provide different ways of generating a wavefront of non-uniform polarization distributions. For the works described thus far, however, the number of polarization channels that can be generated is limited to four. Many applications, such as optical document security, would benefit from a significant increase in the number of polarization states. Wen *et al.*[54] demonstrated this capability by interleaving two types of nanorods to form a single metasurface hologram. As shown in Figs. 7(a) and 7(b), the green and blue nanorods of this reflection-mode metasurface act upon the LCP and RCP components of the illumination. These then form the same pattern but with orthogonal circular polarization states. Since there are displacements of green and blue nanorods in the *x*-direction, a coordinate-related phase difference δ between LCP and RCP holographic images is generated. This in turn results in a coordinate-related polarization distribution [Figs. 7(c)–7(e)]. The technique demonstrated may benefit applications such as the generation of vectorial spot arrays, where each spot possesses a unique polarization state. This could also form the basis for a compact birefringence detector. The vectorial hologram would pass through the birefringence analyte and a fixed polarizer. The birefringence of the sample could then be deduced from the read-out of the image.

It is worth nothing that although continuous polarization distribution means unlimited polarization states, distribution of these states is also "pinned," i.e., the polarization states can only be gradually transformed from *x*- to *y*-, and it is not possible to bypass or recode the intermediate states. In the ideal case, if the phase, amplitude, and polarization of the light reflected or transmitted by a metasurface pixel can be freely modulated, the vectorial holography can be achieved in a more flexible way to realize arbitrary polarization distributions.

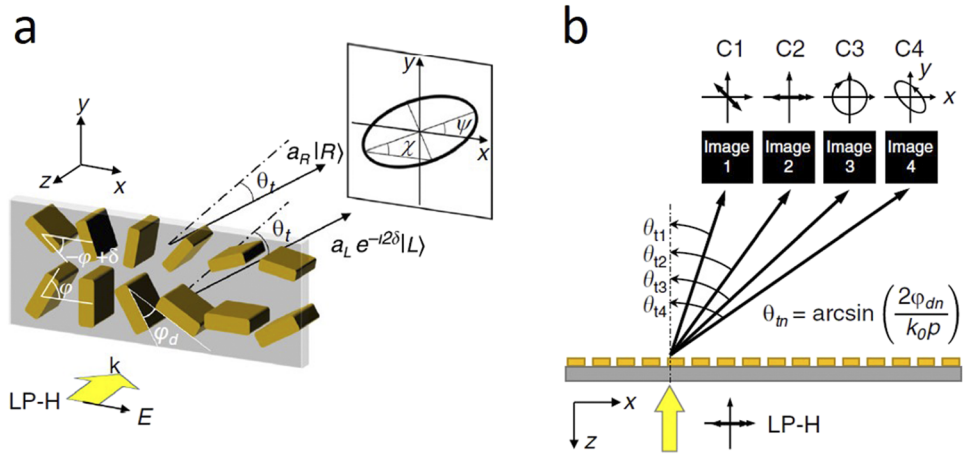

FIG. 6. (a) Schematic of a unit cell. LP-H: linear polarization in the horizontal direction. a_L/a_R: amplitude of the LCP and RCP beams. $|L\rangle$ and $|R\rangle$ represent the left and right-handed circular polarization states, respectively. (b) Multi-directional holographic images with different polarization states. Figures are reproduced with permission from Nat. Commun. **11**, 2651 (2020). Copyright 2020 Springer Nature.

III. INTEGRATION OF A METASURFACE WITH LIGHT SOURCES

One of the key motivations for the development of metasurfaces has been the possibilities that they open up for the miniaturization of optical systems. This stems from the fact that they comprise just a thin layer of nanostructures but can perform the functions normally achieved by one or more bulk optical components. We argue, however, that the benefits for metasurfaces for the realization of miniaturized optical systems are yet to be fully realized as most demonstrations have not miniaturized critical components of such systems such as light sources. In this section, we discuss the important progress that has been made on integrating metasurfaces with lasers to modify the laser output beam. There are typically two ways of doing that, which we term on-facet integration and in-cavity integration. For the former, the metasurfaces are usually located on the emitting surface of the light source. The metasurfaces either provide strong reflection difference to suppress certain modes, or they have minimal effect on the modes in the cavity and instead just modify the wavefront of the beam as it passes through it. For the cases when the metasurfaces are inserted into the cavity and serve as phase or polarization modulators, the field distribution within the cavity can be modified significantly, which in turn changes the properties of the output beam.

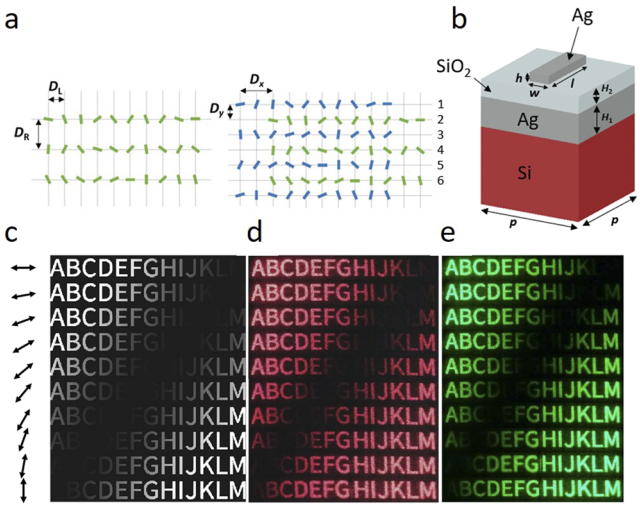

FIG. 7. (a) Schematic of metasurfaces before (left panel) and after (right panel) the interleaving process. (b) The schematic of a unit cell. (c) Simulated holographic images after passing through the analyzing polarizer (black arrow). (d) and (e) Experimental results for illumination with red (λ = 635 nm) and green (λ = 532 nm) lasers. Figures are reproduced with permission from Nano Lett. **21**, 1735–1741 (2021). Copyright 2021 American Chemical Society.

A. Lasers with on-facet metasurfaces

One of the simplest structures that can be integrated with a laser is a linear grating. In 1995, Mukaihara *et al.*[55] demonstrated the control of vertical-cavity surface-emitting laser (VCSEL) polarization with a metal–dielectric grating. The phase of the light reflected from the grating is dependent on the polarization state of the illumination, which makes it possible to have an anti-resonant phase condition for one polarization and a resonant condition for the other. The reflection coefficients of the two polarization states can thus be quite different. In other words, one mode experiences a higher facet reflectance than the other, resulting in lasing occurring on this mode. This in turn controls the output polarization. The grating on the VCSEL can also be made of amorphous silicon[56] or GaAs[57] or can be directly fabricated on the top distributed Bragg reflector (DBR) layer of the VCSEL[58] or in its cap layer.[59] Xu *et al.*[60] demonstrated an approach for dynamically controlling the polarization of a THz VCSEL. This is achieved by incorporating two sets of gratings in the metasurface, each type selectively amplifying a certain polarization mode in the cavity. The two sets of gratings are spatially isolated and can be biased independently; therefore, the polarization states can be actively switched. In addition to using gratings for polarization

control, by varying the nanostructure geometry, such as the ridge width and the period, other functions can be realized, such as focusing[61] and beam shaping.[62] It has even been shown that the three important functionalities, namely, laser feedback, wavelength control, and polarization control, can be achieved simultaneously.[63] Although we mainly focus on gratings on laser facets in this section, it is worth mentioning that they can be integrated with light sources other than lasers. Chen *et al.* demonstrated an InGaN LED that emits linearly polarized white light via the integration of bilayer aluminum gratings.[64] Similar principles can be applied to organic LEDs for white light polarization control.[65]

In 2002, Lezec *et al.*[66] demonstrated that by creating periodic structures around an aperture where the light transmits from, the output beam can have a small angular divergence, i.e., beaming effect. The effect was utilized by Yu *et al.*[67] to realize a small divergence quantum cascaded laser with plasmonic collimators. The collimator contains two functional parts: a slit on the emitting surface couples the laser output into surface plasmons, and the grating patterns adjacent to the slit scatter the surface plasmons into free space. Since the grating area is much larger than the slit widths, a much smaller divergence of the outcoupled radiation will be induced, which is a well-known conclusion in Fourier optics. The rectangle-shaped slit is of sub-wavelength along its short axis, so light incident upon it with polarization across this axis is coupled into surface plasmons on the metal film (in which the slit is situated). This effect can be used for polarization control of the output beam.[68]

Another notable work was as follows: Stellinga *et al.*[69] generated an azimuthally polarized vortex beam from an organic semiconductor laser by patterning the emitting facet with a silicon surface relief grating. The grating was an Archimedean spiral design with a certain number of arms. This resulted in the emitted light being transformed by the grating via the imposition of a vortex phase with the topological charge equal to the arm number. The azimuthally polarized vortex beam with topological charges of 0, 1, 2, and 3 was demonstrated. Li *et al.*[62] fabricated silicon nitride spiral phase plates on a VCSEL for vortex beam generation. The phase varied from 0 to 2π in eight steps, with the phase of each step determined by its thickness. The output beam from the VCSEL is converted by the phase plate into a beam carrying OAM modes. A superposition of multiple OAM states is demonstrated with a concentric spiral phase plate consisting of an inner region and outer region of different topological charges. Sun *et al.*[70] used amorphous silicon nanopillars on the VCSEL emitting surface for OAM generation, where the silicon nanopillars have a fixed height and their diameter and location vary with the designed phase.

Xie *et al.*[71] demonstrated metasurfaces consisting of GaAs nanopillars (500 nm tall) fabricated into a back-emitting VCSEL. The nanopillars are formed by directly etching the GaAs substrate of the VCSEL, i.e., without additional thin film deposition processes. The diameters of the nanopillars are varied to provide phase modulation for the transmitted light in a polarization-independent manner. Transmission efficiency of the metasurface is high (about 80%) and hence barely affects the lasing condition. Remarkable phase control is demonstrated, with various beam profiles, including self-collimated, Bessel, and vortex beams, being generated by the laser.

Wen *et al.* integrated metasurfaces on a VCSEL for simultaneous polarization state generation and detection.[72] Two devices are demonstrated. The first one uses amorphous silicon metasurfaces that provide different phase gradients to the LCP and RCP components of the incident light [Fig. 8(a)]. As a result, the LCP/RCP components of the light from the VCSEL are separated and diverted in different directions [Fig. 8(b)]. When the VCSEL is reverse-biased and the circularly polarized light illuminates the VCSEL at an angle corresponding to the first diffraction order, the detected photocurrent will be related to the handedness of the incident light [Figs. 8(c) and 8(d)]. The second device uses a bilayer aluminum grating that works as a linear polarizer to define the polarization of the output light. When reverse biased, the device acts as a detector, enabling x-/y-polarization states to be distinguished. The fact that polarization generation and detection functions can be achieved in a single device could benefit optical communication systems, such as free-space optical interconnects.

B. Lasers with in-cavity metasurfaces

It is well known that the characteristics of the output beam from a laser can be controlled by inserting engineered optical elements inside the cavity. Early work included the use of intracavity binary amplitude masks,[73,74] phase masks, polarization elements,[75] and so on. Porat *et al.*[76] demonstrated a device for generating an Airy beam from a laser where a 808 nm laser diode was used to pump a 1% Nd:YAG rod to generate a beam at λ = 1064 nm. An aperiodic binary diffraction grating was used as an output coupler. The zeroth order reflected light from the grating was coupled back into the cavity while the −first order was Fourier-transformed by a lens to generate an Airy beam.

Naidoo *et al.*[21] showed that higher-order Poincaré sphere beams can be generated from a laser. As shown in Fig. 9, light with

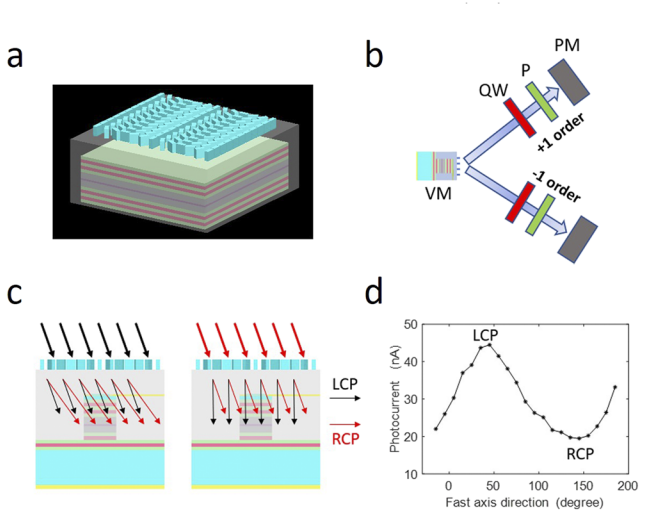

FIG. 8. (a) Schematic of the metasurface integrated with VCSEL. (b) The experimental setup to characterize the polarization state of the output light. VM: VCSEL with a metasurface. QW: quarter wave plate. P: linear polarizer. PM: power meter. (c) The schematic of components of the transmitted beam when incident light is LCP and RCP. (d) Measured photocurrent vs fast axis direction of the quarter wave plate when VCSEL is reverse biased at −2 V. Figures are reproduced with permission from Adv. Opt. Mater. **9**, 2001780 (2021). Copyright 2021 Wiley-VCH GmbH.

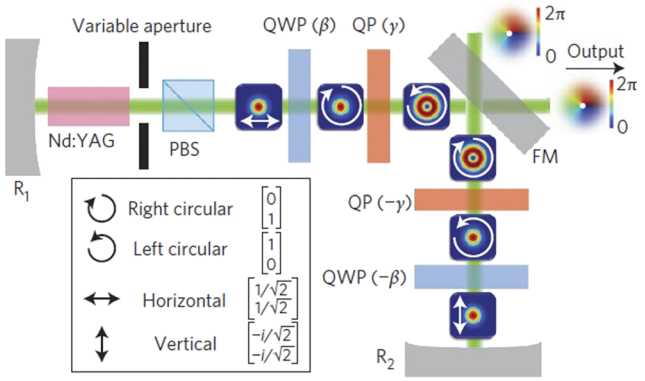

FIG. 9. Experimental setup for generation of higher-order Poincaré sphere beams from a laser. R_1/R_2: end mirrors. PBS: polarizing beam splitter. QWP: quarter-wave plate. QP: q-plate. FM: 45° mirror. Figures are reproduced with permission from Nat. Photonics **10**, 327–332 (2016). Copyright 2016 Springer Nature.

spin angular momentum can be generated via the polarization beam splitter and the quarter-waveplate. The beam then passes through a non-homogeneous polarization optic (q-plate) and is imparted with orbital angular momentum. It is worth noting that another pair of q-plate/quarter-waveplate is located symmetrically in the cavity, which ensures that the polarization states are repeated after each complete round trip. The repeating mode in the cavity is determined by rotation angles of the QWP and q-plate (β and γ). By properly setting the values of β and γ, light beams with pure OAM states and with superposed OAM states (such as radially polarized or azimuthally polarized light or any other points on the Poincaré sphere) can be generated. Maguid *et al.*[77] used a quarter-wave plate, a Faraday rotator, and a linear polarizer to enforce the circular polarization state in the cavity (Fig. 10). The handedness of the circular polarization state in the cavity can be determined by the direction of the quarter waveplate, i.e., setting it to 45° or −45°. When the Faraday rotator and the quarter waveplate are removed, there will be no preference of LCP or RCP, and hence, the $l = 1$ and $l = -1$ modes superpose and form an azimuthally polarized beam.

Huang *et al.*[78] demonstrated a perovskite-based vortex microlaser and verified its ultrafast all-optical switching. The metasurface is composed of circular holes in a 220-nm $MAPbBr_3$ film. One of the TM resonance modes has an appreciable Q-factor in the gain spectral range, representing a bound state in the continuum (BIC) mode with an embedded polarization vortex. When the metasurface is pumped with a circular-shaped incident beam, the vector vortex beam is generated. However, when the pumping condition is changed, for example, the circular-shaped beam is changed to elliptical or two overlapped circular beams are used, the symmetry protection is broken, and two linearly polarized diffracted beams are thus produced.

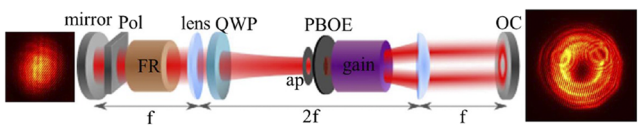

FIG. 10. Schematic of the laser cavity for spin-controlled intracavity mode generation. Pol: polarizer. FR: Faraday rotator. QWP: quarter-wave plate. ap: aperture. PBOE: Pancharatnam–Berry phase optical elements. OC: output coupler. Figures are reproduced with permission from ACS Photonics **5**, 1817–1821 (2018). Copyright 2018 American Chemical Society.

IV. CONCLUSION AND PERSPECTIVE

The field of metasurfaces is rapidly expanding, driven by both scientific interest and industry applications. Indeed, some 1554 papers were published on this topic in 2018, and more than 2000 papers in each of 2019 and 2020 (Web of Science). In this Perspective, we have highlighted what we regard as the two important emerging themes of vectorial holography (to improve metasurfaces' light field modulation capacity) and laser integration. Even though progress has been made, in our opinion, there are several matters that will need to be addressed for this to continue. We discuss these below.

For the metasurfaces that modulate a certain property of light, such as phase or polarization, the modulation depth and conversion efficiency have reached satisfactory levels. For example, Zheng *et al.*[79] demonstrated a reflection-mode geometric metasurface hologram with 16 phase levels, with a maximum efficiency of 80% at 825 nm. Wang *et al.*[80] used silicon nanopillars to modulate the phase of the transmitted light, with the measured efficiency exceeding 90%. However, when metasurfaces are designed to simultaneously modulate two or more parameters of the light field, problems emerge. Although we demonstrated holograms with simultaneous phase and polarization modulation that generate continuous polarization distributions in the observation plane,[54] the measured maximum efficiency is ~17%. This is mainly due to the supercell structure within the metasurface, which distributes energy to multiple diffraction orders except for the ones we are interested in. The low efficiency problem also troubles other metasurface-based vectorial holograms.[50,52] To boost the efficiency, new fabrication techniques/design principles or additional tunable parameters of the unit cell will need to be introduced. As an example, if the pixel size of the metasurface can be reduced with a more refined fabrication technique,[54] we would expect a higher efficiency since some unwanted high diffraction orders can be eliminated.

For most lasers with on-facet metasurfaces, the fabrication process starts from the formation of the laser cavity and then the integration of metasurfaces on the facet. This procedure proves to be difficult since the laser cavity is usually a mesa structure that is above the substrate, e.g., VCSEL, and the emitting surface is usually quite limited in size. A smart method is to fabricate a metasurface on the substrate of back-emitting lasers,[71] which greatly reduces the fabrication difficulty. Although there is no substantial difference between the lasers with on-facet metasurfaces and a tandem system comprising separated lasers and metasurfaces, there is no doubt that the former facilitates integration of the optical systems. The integration method can also be applied to the integration of metasurfaces with other optoelectrical devices such as photodetectors. For lasers with in-cavity metasurfaces, it is possible to generate high purity orbital angular momentum modes due to laser mode competition and purification, which is not achievable through lasers with on-facet metasurfaces. However, the presence of a metasurface in a cavity will change the resonance condition of the cavity,

which induces changes to the lasing mode and threshold. Therefore, metasurfaces with high conversion efficiency and fine adjustment of cavity elements are key factors in realizing such devices.

In this Perspective, we also envision several future development paths of metasurfaces. The first is that of metasurfaces fabricated over large scales and at low cost. Most metasurfaces are currently fabricated with tools such as electron beam lithography or focused ion beam milling. While these have high accuracy, they are likely impractical for large scale production due to their high cost. Several attempts have been made to overcome this difficulty, such as the application of deep ultraviolet (DUV) projection stepper lithography,[81] solution-based deposition techniques,[82] and mask colloidal lithography.[83] The second is that of active metasurfaces. Most metasurfaces demonstrated so far are passive devices, i.e., the function of the metasurface is fixed once it is fabricated. A metasurface whose properties are tunable via external stimuli, such as electrical or optical fields, would be useful for many applications. Great effort has been taken in active metasurfaces in recent years.[84–86] The third is that of quantum metasurfaces. A broad range of novel applications of metasurfaces can find their way to quantum photonics,[87] such as quantum entanglement and single-photon detection.

ACKNOWLEDGMENTS

This work was supported, in part, by the Australian Research Council Centre of Excellence for Transformative Meta-Optical Systems (Project No. CE200100010).

DATA AVAILABILITY

The data that support the findings of this study are available from the corresponding author upon reasonable request.

REFERENCES

[1] S. Sun, K.-Y. Yang, C.-M. Wang, T.-K. Juan, W. T. Chen, C. Y. Liao, Q. He, S. Xiao, W.-T. Kung, G.-Y. Guo, L. Zhou, and D. P. Tsai, "High-efficiency broadband anomalous reflection by gradient meta-surfaces," Nano Lett. **12**, 6223–6229 (2012).

[2] M. Khorasaninejad, W. T. Chen, R. C. Devlin, J. Oh, A. Y. Zhu, and F. Capasso, "Metalenses at visible wavelengths: Diffraction-limited focusing and subwavelength resolution imaging," Science **352**, 1190–1194 (2016).

[3] L. Huang, X. Chen, H. Mühlenbernd, H. Zhang, S. Chen, B. Bai, Q. Tan, G. Jin, K.-W. Cheah, C.-W. Qiu, J. Li, T. Zentgraf, and S. Zhang, "Three-dimensional optical holography using a plasmonic metasurface," Nat. Commun. **4**, 2808 (2013).

[4] F. Aieta, P. Genevet, M. A. Kats, N. Yu, R. Blanchard, Z. Gaburro, and F. Capasso, "Aberration-free ultrathin flat lenses and axicons at telecom wavelengths based on plasmonic metasurfaces," Nano Lett. **12**, 4932–4936 (2012).

[5] F. Ding, Z. Wang, S. He, V. M. Shalaev, and A. V. Kildishev, "Broadband high-efficiency half-wave plate: A supercell-based plasmonic metasurface approach," ACS Nano **9**, 4111–4119 (2015).

[6] K. T. P. Lim, H. Liu, Y. Liu, and J. K. W. Yang, "Holographic colour prints for enhanced optical security by combined phase and amplitude control," Nat. Commun. **10**, 25 (2019).

[7] D. Wen, J. J. Cadusch, J. Meng, and K. B. Crozier, "Multifunctional dielectric metasurfaces consisting of color holograms encoded into color printed images," Adv. Funct. Mater. **30**, 1906415 (2020).

[8] Q. Wei, B. Sain, Y. Wang, B. Reineke, X. Li, L. Huang, and T. Zentgraf, "Simultaneous spectral and spatial modulation for color printing and holography using all-dielectric metasurfaces," Nano Lett. **19**, 8964–8971 (2019).

[9] Y. Bao, Y. Yu, H. Xu, C. Guo, J. Li, S. Sun, Z.-K. Zhou, C.-W. Qiu, and X.-H. Wang, "Full-colour nanoprint-hologram synchronous metasurface with arbitrary hue-saturation-brightness control," Light: Sci. Appl. **8**, 95 (2019).

[10] F. Zhang, M. Pu, P. Gao, J. Jin, X. Li, Y. Guo, X. Ma, J. Luo, H. Yu, and X. Luo, "Simultaneous full-color printing and holography enabled by centimeter-scale plasmonic metasurfaces," Adv. Sci. **7**, 1903156 (2020).

[11] G. Li, S. Chen, N. Pholchai, B. Reineke, P. W. H. Wong, E. Y. B. Pun, K. W. Cheah, T. Zentgraf, and S. Zhang, "Continuous control of the nonlinearity phase for harmonic generations," Nat. Mater. **14**, 607–612 (2015).

[12] G.-Y. Lee, G. Yoon, S.-Y. Lee, H. Yun, J. Cho, K. Lee, H. Kim, J. Rho, and B. Lee, "Complete amplitude and phase control of light using broadband holographic metasurfaces," Nanoscale **10**, 4237–4245 (2018).

[13] L. Liu, X. Zhang, M. Kenney, X. Su, N. Xu, C. Ouyang, Y. Shi, J. Han, W. Zhang, and S. Zhang, "Broadband metasurfaces with simultaneous control of phase and amplitude," Adv. Mater. **26**, 5031–5036 (2014).

[14] Q. Wang, Q. Xu, X. Zhang, C. Tian, Y. Xu, J. Gu, Z. Tian, C. Ouyang, X. Zhang, J. Han, and W. Zhang, "All-dielectric meta-holograms with holographic images transforming longitudinally," ACS Photonics **5**, 599–606 (2018).

[15] A. Arbabi, Y. Horie, M. Bagheri, and A. Faraon, "Dielectric metasurfaces for complete control of phase and polarization with subwavelength spatial resolution and high transmission," Nat. Nanotechnol. **10**, 937–943 (2015).

[16] W. T. Chen, A. Y. Zhu, V. Sanjeev, M. Khorasaninejad, Z. Shi, E. Lee, and F. Capasso, "A broadband achromatic metalens for focusing and imaging in the visible," Nat. Nanotechnol. **13**, 220–226 (2018).

[17] S. Wang, P. C. Wu, V.-C. Su, Y.-C. Lai, M.-K. Chen, H. Y. Kuo, B. H. Chen, Y. H. Chen, T.-T. Huang, J.-H. Wang, R.-M. Lin, C.-H. Kuan, T. Li, Z. Wang, S. Zhu, and D. P. Tsai, "A broadband achromatic metalens in the visible," Nat. Nanotechnol. **13**, 227–232 (2018).

[18] S. Wang, P. C. Wu, V.-C. Su, Y.-C. Lai, C. H. Chu, J.-W. Chen, S.-H. Lu, J. Chen, B. Xu, C.-H. Kuan, T. Li, S. Zhu, and D. P. Tsai, "Broadband achromatic optical metasurface devices," Nat. Commun. **8**, 187 (2017).

[19] J. Meng, J. J. Cadusch, and K. B. Crozier, "Detector-only spectrometer based on structurally colored silicon nanowires and a reconstruction algorithm," Nano Lett. **20**, 320–328 (2019).

[20] Z. Yao, X. Xia, Y. Hou, P. Zhang, X. Zhai, and Y. Chen, "Metasurface-enhanced optical lever sensitivity for atomic force microscopy," Nanotechnology **30**, 365501 (2019).

[21] D. Naidoo, F. S. Roux, A. Dudley, I. Litvin, B. Piccirillo, L. Marrucci, and A. Forbes, "Controlled generation of higher-order Poincaré sphere beams from a laser," Nat. Photonics **10**, 327–332 (2016).

[22] A. W. Lohmann, "Reconstruction of vectorial wavefronts," Appl. Opt. **4**, 1667–1668 (1965).

[23] A. Pors, O. Albrektsen, I. P. Radko, and S. I. Bozhevolnyi, "Gap plasmon-based metasurfaces for total control of reflected light," Sci. Rep. **3**, 2155 (2013).

[24] W. T. Chen, K.-Y. Yang, C.-M. Wang, Y.-W. Huang, G. Sun, I.-D. Chiang, C. Y. Liao, W.-L. Hsu, H. T. Lin, S. Sun, L. Zhou, A. Q. Liu, and D. P. Tsai, "High-efficiency broadband meta-hologram with polarization-controlled dual images," Nano Lett. **14**, 225–230 (2014).

[25] E. Schonbrun, K. Seo, and K. B. Crozier, "Reconfigurable imaging systems using elliptical nanowires," Nano Lett. **11**, 4299–4303 (2011).

[26] A. Martins, J. Li, A. F. da Mota, V. M. Pepino, Y. Wang, L. G. Neto, F. L. Teixeira, E. R. Martins, and B.-H. V. Borges, "Broadband c-Si metasurfaces with polarization control at visible wavelengths: Applications to 3D stereoscopic holography," Opt. Express **26**, 30740–30752 (2018).

[27] Z. Xie, T. Lei, G. Si, X. Wang, J. Lin, C. Min, and X. Yuan, "Meta-holograms with full parameter control of wavefront over a 1000 nm bandwidth," ACS Photonics **4**, 2158–2164 (2017).

[28] C. Min, J. Liu, T. Lei, G. Si, Z. Xie, J. Lin, L. Du, and X. Yuan, "Plasmonic nano-slits assisted polarization selective detour phase meta-hologram," Laser Photonics Rev. **10**, 978–985 (2016).

[29] A. Pors, M. G. Nielsen, and S. I. Bozhevolnyi, "Plasmonic metagratings for simultaneous determination of Stokes parameters," Optica **2**, 716–723 (2015).

[30] M. D. Aiello, A. S. Backer, A. J. Sapon, J. Smits, J. D. Perreault, P. Llull, and V. M. Acosta, "Achromatic varifocal metalens for the visible spectrum," ACS Photonics **6**, 2432–2440 (2019).

[31]S. Boroviks, R. A. Deshpande, N. A. Mortensen, and S. I. Bozhevolnyi, "Multifunctional metamirror: Polarization splitting and focusing," ACS Photonics **5**, 1648–1653 (2017).
[32]F. Cheng, L. Ding, L. Qiu, D. Nikolov, A. Bauer, J. P. Rolland, and A. N. Vamivakas, "Polarization-switchable holograms based on efficient, broadband multifunctional metasurfaces in the visible regime," Opt. Express **26**, 30678–30688 (2018).
[33]T. Todorov, L. Nikolova, K. Stoyanova, and N. Tomova, "Polarization holography. 3: Some applications of polarization holographic recording," Appl. Opt. **24**, 785–788 (1985).
[34]F. Gori, "Measuring Stokes parameters by means of a polarization grating," Opt. Lett. **24**, 584–586 (1999).
[35]Z. Bomzon, G. Biener, V. Kleiner, and E. Hasman, "Space-variant Pancharatnam–Berry phase optical elements with computer-generated subwavelength gratings," Opt. Lett. **27**, 1141–1143 (2002).
[36]D. Wen, F. Yue, G. Li, G. Zheng, K. Chan, S. Chen, M. Chen, K. F. Li, P. W. H. Wong, and K. W. Cheah, "Helicity multiplexed broadband metasurface holograms," Nat. Commun. **6**, 8241 (2015).
[37]F. Yue, X. Zang, D. Wen, Z. Li, C. Zhang, H. Liu, B. D. Gerardot, W. Wang, G. Zheng, and X. Chen, "Geometric phase generated optical illusion," Sci. Rep. **7**, 11440 (2017).
[38]F. Yue, D. Wen, C. Zhang, B. D. Gerardot, W. Wang, S. Zhang, and X. Chen, "Multichannel polarization-controllable superpositions of orbital angular momentum states," Adv. Mater. **29**, 1603838 (2017).
[39]L. Huang, H. Mühlenbernd, X. Li, X. Song, B. Bai, Y. Wang, and T. Zentgraf, "Broadband hybrid holographic multiplexing with geometric metasurfaces," Adv. Mater. **27**, 6444–6449 (2015).
[40]Q. Wei, L. Huang, X. Li, J. Liu, and Y. Wang, "Broadband multiplane holography based on plasmonic metasurface," Adv. Opt. Mater. **5**, 1700434 (2017).
[41]B. Wang, F. Dong, D. Yang, Z. Song, L. Xu, W. Chu, Q. Gong, and Y. Li, "Polarization-controlled color-tunable holograms with dielectric metasurfaces," Optica **4**, 1368–1371 (2017).
[42]L. Jin, Z. Dong, S. Mei, Y. F. Yu, Z. Wei, Z. Pan, S. D. Rezaei, X. Li, A. I. Kuznetsov, and Y. S. Kivshar, "Noninterleaved metasurface for (2^6-1) spin-and wavelength-encoded holograms," Nano Lett. **18**, 8016–8024 (2018).
[43]H. Feng, Q. Li, W. Wan, J.-H. Song, Q. Gong, M. L. Brongersma, and Y. Li, "Spin-switched three-dimensional full-color scenes based on a dielectric metahologram," ACS Photonics **6**, 2910–2916 (2019).
[44]X. Zhang, M. Pu, Y. Guo, J. Jin, X. Li, X. Ma, J. Luo, C. Wang, and X. Luo, "Colorful metahologram with independently controlled images in transmission and reflection spaces," Adv. Funct. Mater. **29**, 1809145 (2019).
[45]G. Li, L. Wu, K. F. Li, S. Chen, C. Schlickriede, Z. Xu, S. Huang, W. Li, Y. Liu, E. Y. B. Pun, T. Zentgraf, K. W. Cheah, Y. Luo, and S. Zhang, "Nonlinear metasurface for simultaneous control of spin and orbital angular momentum in second harmonic generation," Nano Lett. **17**, 7974–7979 (2017).
[46]W. Ye, F. Zeuner, X. Li, B. Reineke, S. He, C.-W. Qiu, J. Liu, Y. Wang, S. Zhang, and T. Zentgraf, "Spin and wavelength multiplexed nonlinear metasurface holography," Nat. Commun. **7**, 11930 (2016).
[47]J. P. Balthasar Mueller, N. A. Rubin, R. C. Devlin, B. Groever, and F. Capasso, "Metasurface polarization optics: Independent phase control of arbitrary orthogonal states of polarization," Phys. Rev. Lett. **118**, 113901 (2017).
[48]R. C. Devlin, A. Ambrosio, N. A. Rubin, J. P. B. Mueller, and F. Capasso, "Arbitrary spin-to-orbital angular momentum conversion of light," Science **358**, 896–900 (2017).
[49]X. Guo, P. Li, B. Li, S. Liu, B. Wei, W. Zhu, J. Zhong, S. Qi, and J. Zhao, "Visible frequency broadband dielectric metahologram by random Fourier phase-only encoding," Sci. China: Phys., Mech. Astron. **64**, 214211 (2021).
[50]R. Zhao, B. Sain, Q. Wei, C. Tang, X. Li, T. Weiss, L. Huang, Y. Wang, and T. Zentgraf, "Multichannel vectorial holographic display and encryption," Light: Sci. Appl. **7**, 95 (2018).
[51]Y. Hu, L. Li, Y. Wang, M. Meng, L. Jin, X. Luo, Y. Chen, X. Li, S. Xiao, H. Wang, Y. Luo, C.-W. Qiu, and H. Duan, "Trichromatic and tripolarization-channel holography with noninterleaved dielectric metasurface," Nano Lett. **20**, 994–1002 (2019).
[52]Z.-L. Deng, J. Deng, X. Zhuang, S. Wang, K. Li, Y. Wang, Y. Chi, X. Ye, J. Xu, G. P. Wang, R. Zhao, X. Wang, Y. Cao, X. Cheng, G. Li, and X. Li, "Diatomic metasurface for vectorial holography," Nano Lett. **18**, 2885–2892 (2018).
[53]Q. Song, A. Baroni, R. Sawant, P. Ni, V. Brandli, S. Chenot, S. Vézian, B. Damilano, P. de Mierry, and S. Khadir, "Ptychography retrieval of fully polarized holograms from geometric-phase metasurfaces," Nat. Commun. **11**, 2651 (2020).
[54]D. Wen, J. J. Cadusch, J. Meng, and K. B. Crozier, "Vectorial holograms with spatially continuous polarization distributions," Nano Lett. **21**, 1735–1741 (2021).
[55]T. Mukaihara, N. Ohnoki, Y. Hayashi, N. Hatori, F. Koyama, and K. Iga, "Polarization control of vertical-cavity surface emitting lasers using a birefringent metal/dielectric polarizer loaded on top distributed Bragg reflector," IEEE J. Sel. Top. Quantum Electron. **1**, 667–673 (1995).
[56]S. J. Schablitsky, L. Zhuang, R. C. Shi, and S. Y. Chou, "Controlling polarization of vertical-cavity surface-emitting lasers using amorphous silicon subwavelength transmission gratings," Appl. Phys. Lett. **69**, 7–9 (1996).
[57]F.-L. Wang, L. Chen, Q.-B. Zhang, L. Xu, H. Li, H.-Z. Wang, Y.-Q. Hao, and X.-H. Ma, "Design of high contrast subwavelength gratings with GaAs-based VCSEL materials," Int. J. Infrared Millimeter Waves **39**, 19–24 (2020).
[58]Q. Wang, Y. Xie, C. Xu, and G. Pan, "Polarization stable VCSEL based on integration of subwavelength gratings with low refractive index medium," in CLEO: QELS_Fundamental Science, 2019.
[59]J. M. Ostermann, P. Debernardi, C. Jalics, A. Kroner, M. C. Riedl, and R. Michalzik, "Surface gratings for polarization control of single-and multimode oxide-confined vertical-cavity surface-emitting lasers," Opt. Commun. **246**, 511–519 (2005).
[60]L. Xu, D. Chen, C. A. Curwen, M. Memarian, J. L. Reno, T. Itoh, and B. S. Williams, "Metasurface quantum-cascade laser with electrically switchable polarization," Optica **4**, 468–475 (2017).
[61]L. Xu, D. Chen, T. Itoh, J. L. Reno, and B. S. Williams, "Focusing metasurface quantum-cascade laser with a near diffraction-limited beam," Opt. Express **24**, 24117–24128 (2016).
[62]K. Li, Y. Rao, C. Chase, W. Yang, and C. J. Chang-Hasnain, "Monolithic high-contrast metastructure for beam-shaping VCSELs," Optica **5**, 10–13 (2018).
[63]M. C. Y. Huang, Y. Zhou, and C. J. Chang-Hasnain, "A surface-emitting laser incorporating a high-index-contrast subwavelength grating," Nat. Photonics **1**, 119–122 (2007).
[64]L. Chen, M. Wang, B. Cao, S. Zhou, Y. Lin, J. Hu, C. Wang, J. Wang, Q. Sun, and K. Xu, "Highly linearly polarized white light emission from InGaN light-emitting diode with nanograting-integrated fluorescent ceramics," Appl. Phys. Express **10**, 012101 (2016).
[65]L. Zhou, Y. Zhou, B. L. Fan, F. Nan, G. H. Zhou, Y. Y. Fan, W. J. Zhang, and Q. D. Ou, "Tailored polarization conversion and light-energy recycling for highly linearly polarized white organic light-emitting diodes," Laser Photonics Rev. **14**, 1900341 (2020).
[66]H. J. Lezec, A. Degiron, E. Devaux, R. A. Linke, L. Martin-Moreno, F. J. Garcia-Vidal, and T. W. Ebbesen, "Beaming light from a subwavelength aperture," Science **297**, 820–822 (2002).
[67]N. Yu, J. Fan, Q. J. Wang, C. Pflügl, L. Diehl, T. Edamura, M. Yamanishi, H. Kan, and F. Capasso, "Small-divergence semiconductor lasers by plasmonic collimation," Nat. Photonics **2**, 564–570 (2008).
[68]N. Yu, Q. J. Wang, C. Pflügl, L. Diehl, F. Capasso, T. Edamura, S. Furuta, M. Yamanishi, and H. Kan, "Semiconductor lasers with integrated plasmonic polarizers," Appl. Phys. Lett. **94**, 151101 (2009).
[69]D. Stellinga, M. E. Pietrzyk, J. M. E. Glackin, Y. Wang, A. K. Bansal, G. A. Turnbull, K. Dholakia, I. D. W. Samuel, and T. F. Krauss, "An organic vortex laser," ACS Nano **12**, 2389–2394 (2018).
[70]Y. Sun, J. Zhu, S. Liu, Y. Yu, and S. Yu, "Direct generation of orbital angular momentum beams by integrating all-dielectric metasurface to vertical-cavity surface-emitting laser," in Asia Communications and Photonics Conference, 2017.
[71]Y.-Y. Xie, P.-N. Ni, Q.-H. Wang, Q. Kan, G. Briere, P.-P. Chen, Z.-Z. Zhao, A. Delga, H.-R. Ren, H.-D. Chen, C. Xu, and P. Genevet, "Metasurface-integrated vertical cavity surface-emitting lasers for programmable directional lasing emissions," Nat. Nanotechnol. **15**, 125–130 (2020).

[72]D. Wen, J. Meng, J. J. Cadusch, and K. B. Crozier, "VCSELs with on-facet metasurfaces for polarization state generation and detection," Adv. Opt. Mater. **9**, 2001780 (2021).
[73]M. Nixon, O. Katz, E. Small, Y. Bromberg, A. A. Friesem, Y. Silberberg, and N. Davidson, "Real-time wavefront shaping through scattering media by all-optical feedback," Nat. Photonics **7**, 919–924 (2013).
[74]M. Nixon, B. Redding, A. A. Friesem, H. Cao, and N. Davidson, "Efficient method for controlling the spatial coherence of a laser," Opt. Lett. **38**, 3858–3861 (2013).
[75]J. Wynne, "Generation of rotationally symmetric TE01 and TM01 modes from a wavelength-tunable laser," IEEE J. Quantum Electron. **10**, 125–127 (1974).
[76]G. Porat, I. Dolev, O. Barlev, and A. Arie, "Airy beam laser," Opt. Lett. **36**, 4119–4121 (2011).
[77]E. Maguid, R. Chriki, M. Yannai, V. Kleiner, E. Hasman, A. A. Friesem, and N. Davidson, "Topologically controlled intracavity laser modes based on Pancharatnam–Berry phase," ACS Photonics **5**, 1817–1821 (2018).
[78]C. Huang, C. Zhang, S. Xiao, Y. Wang, Y. Fan, Y. Liu, N. Zhang, G. Qu, H. Ji, and J. Han, "Ultrafast control of vortex microlasers," Science **367**, 1018–1021 (2020).
[79]G. Zheng, H. Mühlenbernd, M. Kenney, G. Li, T. Zentgraf, and S. Zhang, "Metasurface holograms reaching 80% efficiency," Nat. Nanotechnol. **10**, 308–312 (2015).
[80]L. Wang, S. Kruk, H. Tang, T. Li, I. Kravchenko, D. N. Neshev, and Y. S. Kivshar, "Grayscale transparent metasurface holograms," Optica **3**, 1504–1505 (2016).
[81]J.-S. Park, S. Zhang, A. She, W. T. Chen, P. Lin, K. M. A. Yousef, J.-X. Cheng, and F. Capasso, "All-glass, large metalens at visible wavelength using deep-ultraviolet projection lithography," Nano Lett. **19**, 8673–8682 (2019).
[82]G. M. Akselrod, J. Huang, T. B. Hoang, P. T. Bowen, L. Su, D. R. Smith, and M. H. Mikkelsen, "Large-area metasurface perfect absorbers from visible to near-infrared," Adv. Mater. **27**, 8028–8034 (2015).
[83]N. Odebo Länk, R. Verre, P. Johansson, and M. Käll, "Large-scale silicon nanophotonic metasurfaces with polarization independent near-perfect absorption," Nano Lett. **17**, 3054–3060 (2017).
[84]S. Bang, J. Kim, G. Yoon, T. Tanaka, and J. Rho, "Recent advances in tunable and reconfigurable metamaterials," Micromachines **9**, 560 (2018).
[85]L. Kang, R. P. Jenkins, and D. H. Werner, "Recent progress in active optical metasurfaces," Adv. Opt. Mater. **7**, 1801813 (2019).
[86]Y. Che, X. Wang, Q. Song, Y. Zhu, and S. Xiao, "Tunable optical metasurfaces enabled by multiple modulation mechanisms," Nanophotonics **9**, 4407–4431 (2020).
[87]A. S. Solntsev, G. S. Agarwal, and Y. S. Kivshar, "Metasurfaces for quantum photonics," Nat. Photonics **15**, 327–336 (2021).